Negative Ion Photoelectron Spectroscopy Confirms the Prediction of a Singlet Ground State for the 1,8-Naphthoquinone Diradical

Zheng Yang,[§] David A. Hrovat,[†] Gao-Lei Hou,[§] Weston Thatcher Borden[*†] and Xue-Bin Wang[*§]

[§]*Physical Sciences Division, Pacific Northwest National Laboratory, P. O. Box 999, MS K8-88, Richland, WA 99352, USA*

[†]*Department of Chemistry and the Center for Advanced, Scientific Computing and Modeling, University of North Texas, 1155 Union Circle, #305070, Denton, Texas 76203-5070, USA*

Corresponding Authors

Xue-Bin Wang: Xuebin.wang@pnnl.gov

Weston T. Borden: Weston.Borden@unt.edu

Abstract

Negative ion photoelectron (NIPE) spectra, with 193, 266, 300, and 355 nm photons, of the radical anion of 1,8-naphthoquinone (1,8-**NQ**$^{\bullet -}$) have been obtained at 20K. The electron affinity of 1,8-**NQ** is determined from the first resolved peak in the NIPE spectrum to be 2.98 ± 0.04 eV. Franck-Condon factors (FCFs), calculated from the CASPT2/aug-cc-pVDZ optimized geometries, normal modes, and vibrational frequencies successfully simulate the intensity and frequencies of the spectral features that are associated with the lowest two electronic states. The NIPE spectra of 1,8-**NQ**$^{\bullet -}$ and the peak assignments, based on the computed FCFs, confirm the theoretical predictions that $^1A_1$ is the ground state of 1,8- **NQ** and that $^3B_2$ is the first excited state. The spectra provide an experimental value of ΔE_{ST} = -1.5 kcal/mol, which is within about 1 kcal/mol of the (12/12)CASPT2/aug-cc-pVTZ calculated value of ΔE_{ST} = -2.6 kcal/mol.

Introduction

The single-triplet energy separations in diradicals have been of interest for many decades.[1-12] Among the diradicals that have been studied, the isomeric benzoquinones (**BQs**) have been of particular interest.[13-20] Both *o*- and *p*-**BQ** have a singlet ground state; whereas, the ground state of *m*-**BQ** is a triplet. A triplet ground state for *m*-**BQ** was first predicted computationally[14] and then confirmed experimentally by negative ion photoelectron (NIPE) spectroscopy of the corresponding radical anion (*m*-**BQ**$^{\bullet-}$).[18,20]

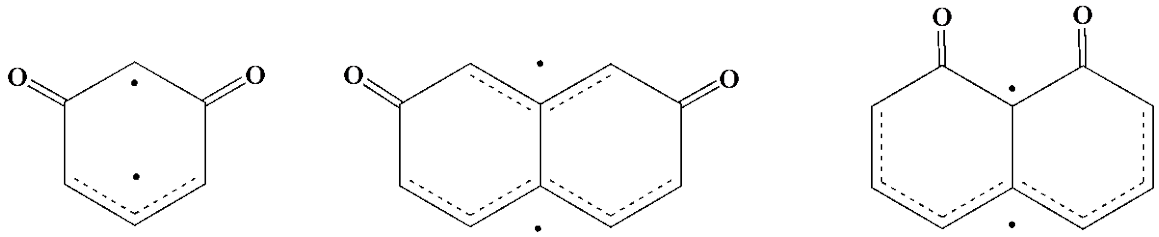

m-**BQ** 2,7-**NQ** 1,8-**NQ**

Figure 1. The structures of the *meta*-benzoquinone (*m*-**BQ**), 2,7-naphthoquinone (2,7-**NQ**), and 1,8-naphthoquinone (1,8-**NQ**) diradicals.

The NIPE spectra of *o*- and *p*-**BQ**$^{\bullet-}$ each reveal a broad ground-state feature and a large band gap, followed by well-resolved excited state peaks, in the neutral molecule.[18] In contrast, the NIPE spectrum of *m*-**BQ**$^{\bullet-}$ is distinctly different from those of its two isomers, showing no clear band gap, a much higher electron affinity (EA) (2.89 eV), and a triplet ground state.[18,20] Calculations not only predicted the triplet ground state of *m*-**BQ** but also the relative energies of the low-lying singlet electronic states of *m*-**BQ**.[14] These predictions were confirmed by the good agreement between Franck-Condon simulations of the NIPE spectrum of *m*-**BQ**$^{\bullet-}$ and the experimental spectrum.[20]

The 2,7-naphthoquinone (2,7-**NQ**) diradical has also been studied both theoretically and experimentally.[21,22] A triplet ground state ($^3B_2$) was predicted by CASPT2 calculations,[21] and this prediction was subsequently confirmed by NIPE spectroscopy on the corresponding radical anion (2,7-**NQ**$^{\bullet-}$).[22]

It would be natural to assume that the isomeric 1,8-naphthoquinone (1,8-**NQ**) diradical also has a triplet ground state. Like 2,7-**NQ**, 1,8-**NQ** is a non-Kekulé quinone, (i.e, a quinone for which no Kekulé structures can be written that do not contain at least two unpaired electrons).[23] However, a recent theoretical study made the surprising prediction that 1,8-**NQ** differs from 2,7-**NQ** by not having a triplet ground state.[24] Instead the ground state of 1,8-**NQ** was predicted to be a singlet ($^1A_1$), with the lowest triplet ($^3B_2$) state calculated to be 2.6 kcal/mole higher in energy.

The reason for this surprising prediction is that, of the two MOs that are singly occupied in the triplet state of 1,8-**NQ**, the b_1 π MO is calculated to be considerably lower in energy than the a_2 π MO. This energy difference, which is computed to amount to 19.5 kcal/mol in the 1,8-**NQ** radical anion (1,8-**NQ**$^{\bullet-}$), is a consequence of the fact that, as shown in Figure 2, the b_1 π MO has one fewer nodal plane than the a_2 π MO. As a result, the double occupancy of the b_1 π MO in the lowest singlet state is computed to be favored over the single occupancy of the b_1 and a_2 π MOs in the lowest triplet state.

The calculations make another interesting prediction. The proximity of the two oxygen atoms in 1,8-**NQ** results in the out-of-phase combination of the two oxygen 2p-σ AOs in the b_2 σ MO destabilizing this MO. This MO, which is also shown in Figure 2, is calculated to be higher in energy (by 6.8 kcal/mol in 1,8-**NQ**$^{\bullet-}$) than the b_1 π MO.

The exchange integral between two π MOs is much larger than that between a σ and a π MO; so the lowest triplet state of 1,8-**NQ** is $^3B_2$, which has the b_2 σ MO doubly occupied and the unpaired electrons in the b_1 and a_2 π MOs. Nevertheless, the lower one-electron energy of the b_1 π MO than of the b_2 σ MO makes the energy computed for the $^3B_1$ state, in which the b_1 π MO is doubly occupied and the unpaired electrons occupy the b_2 σ and a_2 π MOs, only 6.0 kcal/mol higher than that of the $^3B_2$ state of 1,8-**NQ**.

Thus, unlike the case in 2,7-**NQ**,[21,22] calculations predict that not only should 1,8-**NQ** have a singlet ground state but there should be a second triplet state that is very close in energy to the lowest triplet state.[24] The NIPES experiments described in this paper were undertaken in order to verify these two predictions.

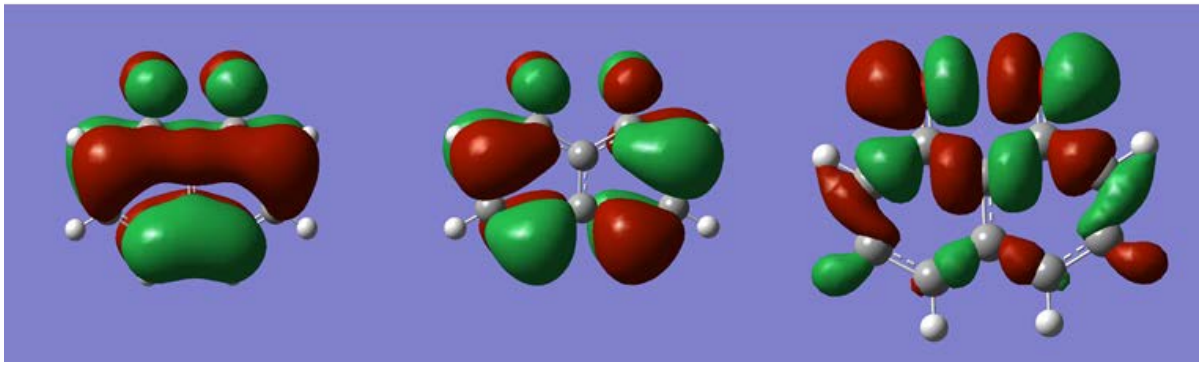

Figure 2. The b_1 (left) and a_2 (center) π MOs and the b_2 (right), oxygen, 2p-σ lone-pair MO of 1,8-**NQ**. The b_2 σ MO and the a_2 π MO are calculated to be, respectively, 6.8, and 19.5 kcal/mol higher in energy than the b_1 π MO in 1,8-**NQ**$^{\bullet -}$.[24]

Experimental Methodology

The negative ion photoelectron spectroscopy (NIPES) experiments were carried out at PNNL using an apparatus consisting of an electrospray ionization (ESI) source, a temperature controlled cryogenic ion trap, and a magnetic-bottle time-of-flight (TOF) photoelectron spectrometer.[25] A 0.1 mM acetonitrile solution of 1,8-dihydroxynaphalene, titrated with a small amount of NaOH dissolved in water, was prepared in a N_2 glovebox, and used to generate 1,8-**NQ**$^{\bullet -}$ by electrospray under an N_2 atmosphere. The ESI conditions were optimized to ensure that the doubly deprotonated species, 1,8-**NQ**$^{\bullet -}$, was a prominent peak in the mass spectrum.

The ions generated by ESI were guided by quadrupole ion guides into the ion trap, where they were accumulated and cooled for 20 – 100 ms by collisions with cold buffer gas (20% H_2 balanced in helium) at 20 K, before being transferred into the extraction zone of a TOF mass spectrometer. The cooling of the anions to 20 K improved the spectral energy resolution and minimized the possibility of the appearance of peaks in the NIPE spectra resulting from hot bands.

The 1,8-**NQ**$^{\bullet -}$ ions were then mass selected and maximally decelerated before being photodetached. In the current study, photon energies of 193 nm (6.424 eV) from an excimer laser, 266 nm (4.661 eV) and 355 nm (3.496 eV) from a Nd:YAG laser, and 300 nm (4.133 eV) from doubling frequency of 600 nm photons from an OPO/OPA laser

were used. The lasers were operated at a 20 Hz repetition rate, with the ion beam off at alternating laser shots, in order to enable shot-to-shot background subtraction.

Photoelectrons were collected with ca. 100% efficiency with the magnetic bottle and analyzed in a 5.2 m long electron-flight tube. The recorded TOF photoelectron spectrum was converted into an electron kinetic-energy spectrum by calibration with the known NIPE spectra of I^- [26] and $OsCl_6^{2-}$.[27] The electron-binding energy (EBE) was obtained by subtracting the electron kinetic energy from the energy of the detaching photons. The energy resolution was about 2% (i.e., ~20 meV for 1 eV kinetic-energy electrons).

Computational Methodology

The geometries, normal modes, and frequencies of 1,8-**NQ** and 1,8-**NQ**$^{\bullet-}$ were calculated at the CASPT2/aug-cc-pVDZ level of theory[28,29] using the MOLCAS (version 8.0) suite of programs.[30] An active space that correlated 12 or 13 electrons in the twelve π-MOs was used for electronic states in which the b_2 σ MO was doubly occupied. For electronic states in which the b_2 σ MO was singly occupied a fourteen orbital active space was used in which 16 or 17 electrons were correlated in the two p-σ lone pair MOs on oxygen in addition to the 12 π-MOs.[24] Franck-Condon factors (FCFs), including Duschinsky rotations, were calculated from the CASPT2/aug-cc-pVDZ optimized geometries, normal modes, and frequencies for totally symmetric (a_1) vibrations, using the ezSpectrum (version 3.0) program, developed by Mozhayskiy and Krylov.[31]

Results and Discussion

Photoelectron spectrum of 1,8-NQ$^{\bullet-}$

The NIPE spectrum of 1,8-**NQ**$^{\bullet-}$ with 266nm photon is shown in Figure 3. The spectra from other photon energies are provided in the Supporting Information in Figure S1.

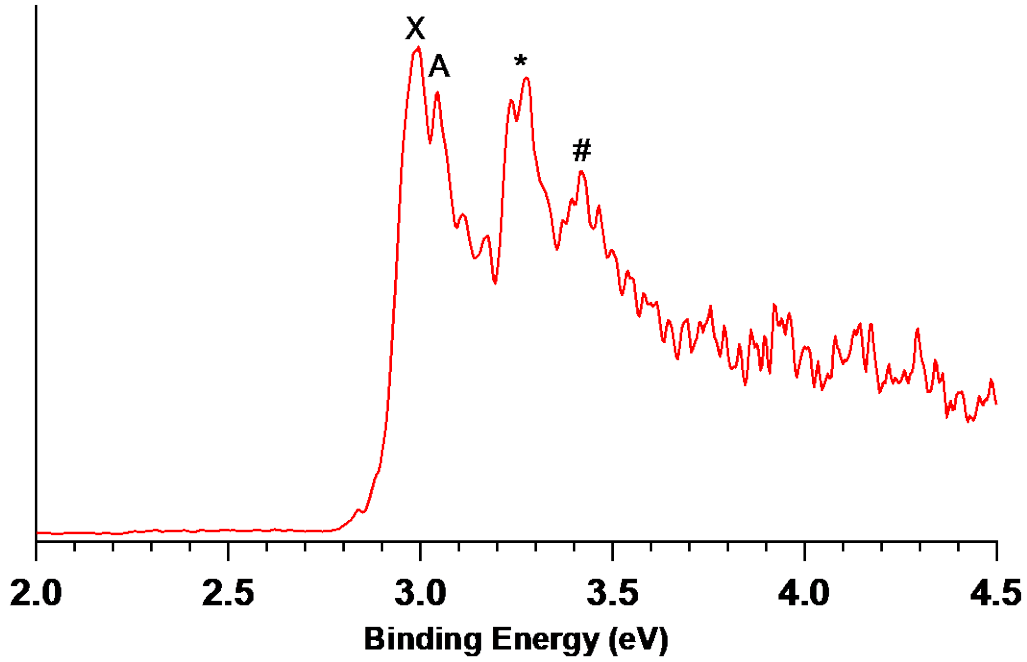

Figure 3. The 20 K NIPE spectrum of 1,8-**NQ**$^{\bullet-}$ at 266 nm.

Several sharp features are seen in the spectrum in the EBE range from c.a. 2.9 eV to 3.5 eV. The lowest energy and highest intensity peak is at EBE 2.98 eV and marked as X. Next to it at EBE 3.045 eV is a slightly lower intensity peak, marked as A. At EBE 3.24 eV and 3.42 eV are two strong features, marked as * and #, respectively. The spectrum becomes an unresolved continuum band after #. The tiny peak at ~2.85 eV is from an unknown impurity.

Assignment of the NIPE spectrum and Discussion

According to the previous CASPT2 calculations,[24] there are five low-lying electronic states of 1,8-**NQ** that might be observed in the NIPE spectrum of 1,8-**NQ**$^{\bullet-}$. These states and their CASPT2 energies, relative to the $^2A_2$ state of 1,8-**NQ**$^{\bullet-}$ are listed in Table 1.

Table 1. The assignments of the major peaks in the NIPE spectrum of 1,8-**NQ**$^{\bullet-}$ and the experimental electron binding energy (*EBE*) (eV) of each. The CASPT2/aug-cc-pVTZ relative energies (ΔE in eV) of the low-lying electronic states of 1,8-**NQ**$^{\bullet-}$ and 1,8-**NQ** from ref. 24 are given for comparison with the experimental binding energies.

Species	Electronic State	ΔE (CASPT2, eV)	NIPES *EBE* (eV)
1,8-**NQ**$^{\bullet-}$	$^2A_2 = \|\ldots b_2^2\ b_1^2 a_2^{\alpha}\rangle$	0	0
1,8-**NQ**	$^1A_1 = c_1\|\ldots b_2^2 b_1^2\rangle - c_2\|\ldots b_2^2 a_2^2\rangle$	2.957[a]	X, 2.98
	$^3B_2 = \|\ldots b_2^2 b_1 a_2(\alpha\beta + \beta\alpha)/\sqrt{2}\rangle$	3.070[a]	A, 3.045
	$^3B_1 = \|\ldots b_1^2 b_2 a_2(\alpha\beta + \beta\alpha)/\sqrt{2}\rangle$	3.330[b]	*, 3.24
	$^1B_1 = \|\ldots b_1^2 b_2 a_2(\alpha\beta - \beta\alpha)/\sqrt{2}\rangle$	3.408[b]	#, 3.42
	$^1B_2 = \|\ldots\ b_2^2 b_1 a_2(\alpha\beta - \beta\alpha)/\sqrt{2}\rangle$	4.133[a]	> 3.5

[a] (12/12)CASPT2/aug-cc-PVTZ//(12/12)CASPT2/aug-cc-PVDZ

[b](16/14)CASPT2/aug-cc-pVTZ//(16/14)CASPT2/aug-cc-pVDZ, combined with the CCSDT/aug-cc-pVTZ energy difference of 0.26 eV between $^3B_1$ and $^3B_2$.

The CASPT2 calculations predict that the $^1A_1$ state is the ground state of 1,8-**NQ**; and just 0.1 eV higher is the $^3B_2$ state. The $^3B_1$ state is calculated to have *EBE* = 3.330 eV, and the $^1B_1$ state is computed to be less than 0.1 eV higher than $^3B_1$. The small exchange energy between electrons in the $b_2\,\sigma$ MO and the $a_2\,\pi$ MO is responsible for the small calculated energy difference between the $^3B_1$ and $^1B_1$ states.[24] The much larger exchange energy between electrons in the $b_1\,\pi$ MO and the $a_2\,\pi$ MO is responsible for the much greater calculated energy difference of 1.06 eV between the $^3B_2$ and $^1B_2$ states.

Comparing the CASPT2 results with the experimental spectrum, we assign peak X at 2.98 eV to the $^1A_1$ state, and peak A at 3.045 to the nearby $^3B_2$ state. The adiabatic CASPT2 energy difference between $^2A_2$ and $^3B_2$, when combined with the CCSD(T) adiabatic energy difference of 0.26 eV between $^3B_2$ and $^3B_1$ gives a predicted *EBE* = 3.33 eV for $^3B_1$, which is in reasonable agreement with the *EBE* = 3.24 for peak * in the NIPE spectrum. As shown in Table 1, peak # can be assigned to the $^1B_1$ state.

Franck-Condon Simulation of the NIPE spectra

In order to further confirm the assignment of the electronic states of 1,8-**NQ** in the NIPE spectrum of 1,8-**NQ**$^{\bullet-}$, the Franck-Condon factors (FCFs) for the transitions from the $^2A_2$ state of 1,8-**NQ**$^{\bullet-}$ to each of the low-lying states of 1,8-**NQ** were calculated, using ezSpectrum.[31] The simulated stick spectrum was convoluted with Gaussian line broadening of the FCFs sticks for each transition. The results are shown in Figure 4, where they have been superimposed on the 266 nm spectrum for comparison. The simulated spectra are shown, superimposed on the experimental 355 nm, 300 nm, and 193 nm NIPE spectra in Figure S1 of the Supporting Information.

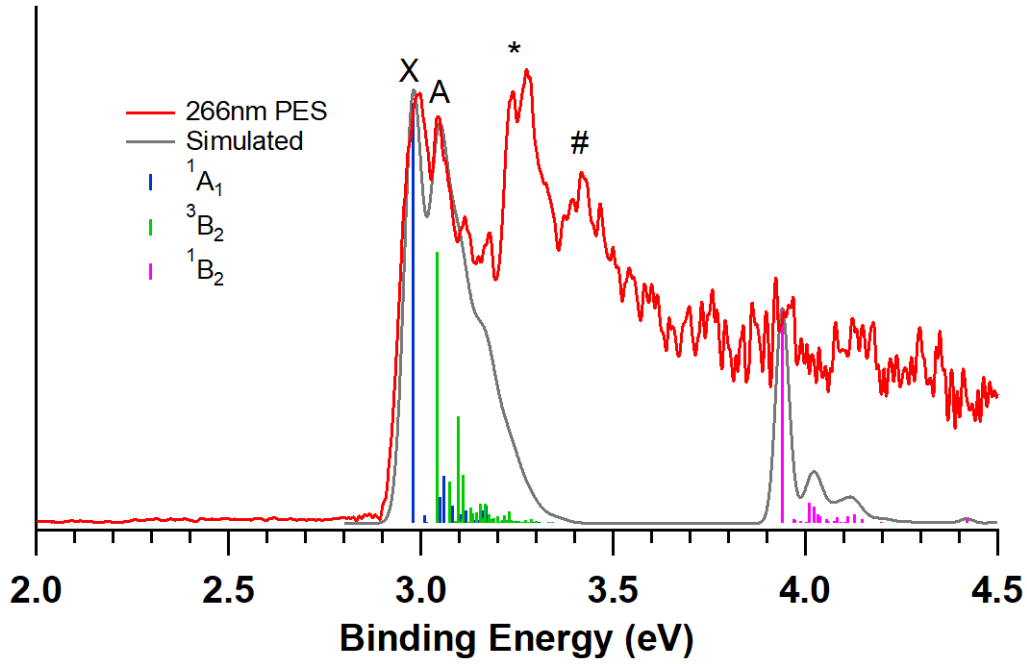

Figure 4. Simulated NIPE spectra for formation of the low-lying electronic states of 1,8-**NQ**, from 1,8-**NQ**$^{\bullet-}$ using the calculated CASPT2/aug-cc-pVDZ stick spectra, convoluted with Gaussian line broadening. The simulated spectra are superimposed onto the experimental spectrum of 1,8-**NQ**$^{\bullet-}$ at 266 nm. The simulated peak intensities and positions of the 0-0 bands have been adjusted to match those in the experimental spectrum. The FWHMs of Gaussians for $^1A_1$, $^3B_2$, and $^1B_2$ peaks are set to 55, 55, and 40 meV. The small peak of impurity at ~2.85 eV was eliminated by background subtraction. No intensity is predicted by the FCFs for the transitions from the $^2A_2$ state of 1,8-**NQ**$^{\bullet-}$ to either the $^3B_1$ or $^1B_1$ states of 1,8-**NQ**.

Due to the small geometry change from $^2A_2$ to $^1A_1$,[24] the 0-0 peak for this electronic transition has the highest intensity in Figure 4. The FCFs decrease quickly for the rest of the vibrational peaks for $^2A_2 \rightarrow {}^1A_1$, and the FCFs are consistent with the assignment of peak X to this transition.

The remaining vibrational peaks for $^2A_2 \rightarrow {}^1A_1$ contribute to the intensity of peak A in the NIPE spectrum. The intensity of peak A would be too low, if it were due entirely to the (0,0) vibrational peak for $^2A_2 \rightarrow {}^3B_2$ state. As shown in Figure 4, the FCFs provide simulated shapes for the first two peaks in the NIPE spectrum of 1,8-**NQ**$^{\bullet-}$ that are consistent with the assignments, based on the *EBE*s in Table 1.

As shown in Table 1, the *EBE*s of peaks * and # in the NIPE spectra in Figures 3 and 4 align well with the *EBEs* computed for formation of the $^3B_1$ and $^1B_1$ states of 1,8-**NQ**. These peaks are intense and appear to come from electronic transitions that have large FCFs. However, the FCFs for formation of the $^3B_1$ and $^1B_1$ states of 1,8-**NQ** from the $^2A_2$ state of 1,8-**NQ**$^{\bullet-}$ are not calculated to be large. They are, in fact, calculated to be zero!

There is a good physical reason why the FCFs are computed to be zero. The transitions from $^2A_2$ to $^3B_1$ and $^1B_1$ involve the loss of an electron from the b_2 σ MO. As shown in Figure 2, this MO is strongly O-O antibonding. Consequently, these transitions result in a huge decrease of ~0.6 Å in the O-O distance. As a result there is no overlap between some of the vibrational wave functions of the $^2A_2$ state of 1,8-**NQ**$^{\bullet-}$ and the corresponding vibrational wave functions of the $^3B_1$ and $^1B_1$ states of 1,8-**NQ**.

Why, then, do peaks * and #, whose *EBEs* correspond closely to those computed for $^3B_1$ and $^1B_1$, have large intensities? An attractive explanation is that these peaks arise from a transition from the $^2A_2$ ground state of 1,8-**NQ**$^{\bullet-}$ to the $^2B_2$ excited state, which is computed to be higher by 13.2 kcal/mol.[24] Like the $^3B_1$ and $^1B_1$ states of 1,8-**NQ**, the $^2B_2$ excited state of 1,8-**NQ**$^{\bullet-}$ has only one electron in the b_2 σ MO; so the O-O distance in $^2B_2$ of 2.241 Å is very close to the O-O distances of 2.201 and 2.232 Å in the $^3B_1$ and $^1B_1$ states, respectively. Consequently, the FCFs for $^2B_2 \rightarrow {}^3B_1$ and $^1B_1$, unlike those for $^2A_2 \rightarrow {}^3B_1$ and $^1B_1$, should be far from zero.

In order to confirm that this is, indeed, the case, we have computed the FCFs for $^2B_2 \rightarrow {}^3B_1$ and $^1B_1$. The resulting vibrational peaks are shown in Figure 5, superimposed on the experimental NIPE spectrum.

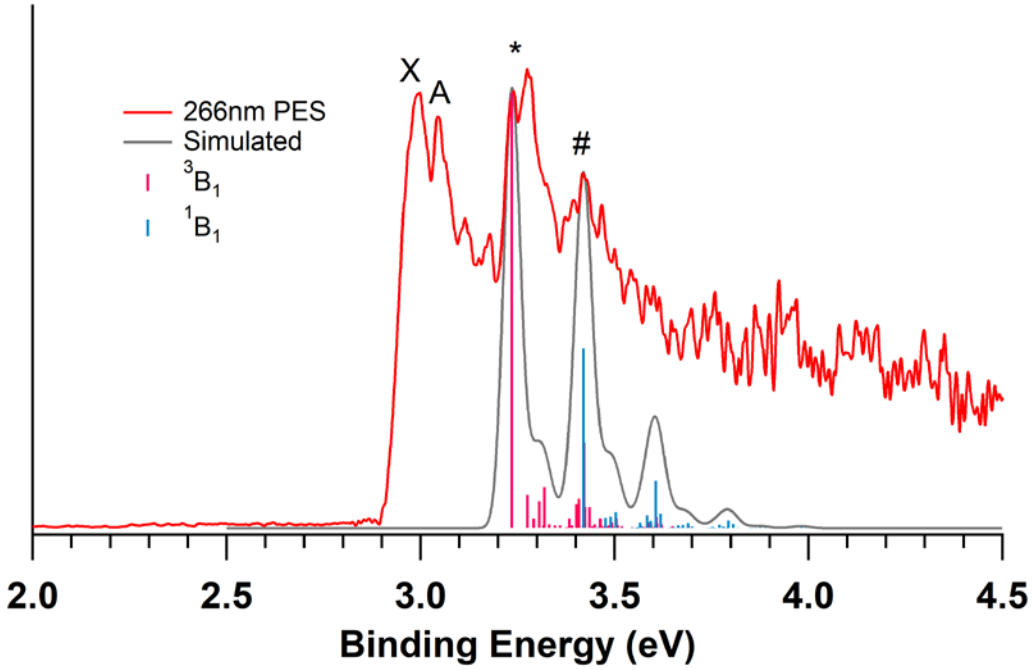

Figure 5. Simulated spectrum for a transition from the $^2B_2$ excited state of 1,8-**NQ**$^{\bullet-}$ to the $^3B_1$ and $^1B_1$ excited states of 1,8-**NQ**, using the calculated CASPT2/aug-cc-pVDZ stick spectra, convoluted with Gaussian line broadening with the FWHMs of Gaussians set to 50 meV. The simulated spectrum containing all five states, i.e., $^1A_1$, $^3B_2$, $^3B_1$, $^1B_1$, and $^1B_2$, superimposed onto the experimental 266 nm spectrum of 1,8-**NQ**$^{\bullet-}$, is provided in Figure S2 of the Supporting Information.

Of course, the *EBE*s for $^2A_2 \rightarrow {}^2B_2$, followed by resonant autodetachment of the $^2B_2$ excited state of 1,8-**NQ**$^{\bullet-}$ to the $^3B_1$ and $^1B_1$ states of 1,8-**NQ** are exactly the same as the *EBE*s for formation of these two states of 1,8-**NQ** directly from the $^2A_2$ state of 1,8-**NQ**$^{\bullet-}$. Consequently, the FCF simulations of the vibrational structure for the formation of the $^3B_1$ and $^1B_1$ states of 1,8-**NQ** are shown in Figure 5 under the * and # peaks, to which these states of 1,8-**NQ** are assigned.

The proposal that resonant autodetachment is responsible for formation of peaks * and # in the NIPE spectrum of 1,8-**NQ**$^{\bullet-}$ is supported by the fact that resonant

autodetachment has been frequently observed in anions of aromatic molecules.[16,22,32] The intensities of the peaks formed by resonant autodetachment have been found to be highly dependent on the photon energy; and, indeed, as can be seen in Figure S1, the intensities of peaks * and # do change a lot with different photon energies. In fact, in the 193 nm NIPE spectrum of 1,8-**NQ**$^{\bullet-}$, it appears that there are no peaks at the positions of * and # seen in the 266 nm and 300 nm NIPE spectra.

Summary and Conclusions

The NIPE spectrum of 1,8-**NQ**$^{\bullet-}$ has confirmed the theoretical prediction that a singlet is the ground state of 1,8-**NQ**. In addition to the very good agreement between the calculated and observed *EBE*s of the first two peaks in the NIPE spectrum, the FCFs, calculated from the CASPT2/aug-cc-pVDZ optimized geometries, normal modes, and frequencies successfully simulated the appearance of these two peaks, with peak X being assigned to the $^1A_1$ ground state, and peak A being assigned to the $^3B_2$ excited state of 1,8-**NQ**.

Peak X has *EBE* = 2.98 eV, and peak A has *EBE* = 3.045 eV. Thus, the experimental value of ΔE_{ST} in 1,8-**NQ** is - 0.065 eV (-1.5 kcal/mole), which is in reasonably good agreement with the predicted value -2.6 kcal/mole.[24]

The next two peaks, * and #, in the NIPE spectrum can be assigned to, respectively, the $^3B_1$ and $^1B_1$ states of 1,8-**NQ**, on the basis of the good correspondence between the *EBE*s measured for these two peaks and those computed for the $^3B_1$ and $^1B_1$ states. Because these two states each have only one electron in the O-O antibonding b_2 MO, these states have much smaller O-O distances than the $^2A_2$ ground state of 1,8-**NQ**$^{\bullet-}$. Consequently, the calculated FCFs for $^2A_2 \rightarrow {}^3B_1$ and $^1B_1$ are zero.

Formation of $^3B_1$ and $^1B_1$ from $^2A_2$ is postulated to occur via an indirect pathway, involving excitation of the $^2A_2$ ground state of 1,8-**NQ**$^{\bullet-}$ to the low-lying $^2B_2$ excited state, which undergoes resonant autodetachment to form $^3B_1$ and $^1B_1$. Because, like the $^3B_1$ and $^1B_1$ states of 1,8-**NQ**, the $^2B_2$ state of 1,8-**NQ**$^{\bullet-}$ has only one electron in the O-O antibonding b_2 MO, the FCFs for $^2B_2 \rightarrow {}^3B_1$ and $^1B_1$ are non-zero. Experimental evidence

for the operation of this resonant autodetachment pathway to form $^3B_1$ and $^1B_1$, comes from the dependence of the intensities of the * and # peaks in the NIPE spectrum of 1,8-**NQ**$^{\bullet-}$ on the energy of the laser used for electron detachment.

Acknowledgement

WTB acknowledges the generous support of his research by Grant B0027 from the Robert A. Welch Foundation and dedicates this paper to Prof. Helmut Schwarz on the occasion of his 75th birthday. The photoelectron spectroscopy work done at PNNL was supported by U.S. Department of Energy (DOE), Office of Science, Office of Basic Energy Sciences, Division of Chemical Sciences, Geosciences, and Biosciences (XBW), and performed in EMSL, a national scientific user facility sponsored by DOE's Office of Biological and Environmental Research and located at Pacific Northwest National Laboratory, which is operated by Battelle Memorial Institute for the DOE.

References

1. Salem, L.; Rowland, C. The Electronic Properties of Diradicals. *Angew. Chem., Int. Ed.* **1972**. *11*, 92-111.
2. Borden, W.T. Ed. *Diradicals*, **1982**, Wiley-Interscience, New York, 1982.
3. Osamura, Y.; Borden, W.T.; Morokuma, K. Structure and Stability of Oxyallyl. An MCSCF Study. *J. Am. Chem. Soc.* **1984**. *106,* 5112-5115.
4. Coolidge, M. B.; Yamashita, K.; Morokuma, K.; Borden, W. T. Ab initio MCSCF and CI Calculations of the Singlet-Triplet Energy Differences in Oxyallyl and in Dimethyloxyallyl. *J. Am. Chem. Soc.* **1990**. *112*,1751-1754.
5. Ervin, K. M.; Lineberger, W.C. in *Advances in Gas Phase Ion Chemistry*. **1992**, JAI Press: Greenwich. p. 121-166.
6. Wenthold, P.G.; Hu, J.; Squires, R. R.; Lineberger, W. C. Photoelectron Spectroscopy of the Trimethylenemethane Negative Ion. The Singlet−Triplet Splitting of Trimethylenemethane. *J. Am. Chem. Soc.* **1996**. *118,* 475-476.

7. Wenthold, P.G.; Kim, J.B.; Lineberger, W.C. Photoelectron Spectroscopy of *m*-Xylylene Anion. *J. Am. Chem. Soc.***1997**. *119*, 1354-1359.
8. Ichino, T.; Villano, S. M.; Gianola, A. J.; Goebbert, D. J.; Velarde, L.; Sanov, A.; Blanksby, S. J.; Zhou, X.; Hrovat, D. A.; Borden, W. T.; Lineberger, W. C. The Lowest Singlet and Triplet States of the Oxyallyl Diradical. *Angew. Chem., Int. Ed.* **2009**. *48*, 8509-8511.
9. Lineberger, W. C.; Borden, W. T. The Synergy between Qualitative Theory, Quantitative Calculations, and Direct Experiments in Understanding, Calculating, and Measuring the Energy Differences between the Lowest Singlet and Triplet States of Organic Diradicals. *Phy. Chem. Chem. Phys.* **2011**. *13*,11792-11813.
10. Abe, M. Diradicals. *Chem. Rev*. **2013**. *113*, 7011-7088.
11. Hrovat, D. A.; Hou, G. L.; Wang, X. B.; Borden, W. T. 2015. Negative Ion Photoelectron Spectroscopy Confirms the Prediction that 1,2,4,5-Tetraoxatetramethylenebenzene Has a Single Groud. *J. Am. Chem. Soc*. **2015**, *137*, 9094-9099.
12. Borden, W.T. *Diradicals – A Fifty Year Fascination*, in *The Foundations of Physical Organic Chemistry: Fifty Years of the James Flack Norris Award*. **2015**, American Chemical Society. p. 251-303.
13. Marks, J.; Comita, P. B.; Brauman, J. I. Threshold Resonances in Electron Photodetachment Spectra. Strcutural Evidence for Dipole-Supported States. *J. Am. Chem. Soc*. **1985**, *107*, 3718-3719.
14. Fort, R. C. Jr.; Getty, S. J.; Hrovat, D. A.; Lahti, P. M.; Borden, W. T. Ab Initio Calculations on *m*-Quinone. The Ground State Is a Triplet. *J. Am. Chem. Soc*. **1992**. *114*, 7549-7552.
15. Itoh, T. Low-Lying Electronic States, Spectroscopy, and Photophysics of Linear Para Acenequinones. *Chem. Rev*. **1995**, *95*, 2351-2368.
16. Schiedt, J.; Weinkauf, R. Resonant Photodetachment via Shape and Feshbach Resonances: *p*-Benzoquinone Anions as a Model System. *J. Chem. Phys.* **1999**, *110*, 304-314.
17. Fattahi, A.; Kass, S. R.; Liebman, J. F.; Matos, M. A. R.; Miranda, M. S.; Morais, V. M. F. The Enthalpies of Formation of *o*-, *m*-, and *p*-Benzoquinone: Gas-Phase

Ion Energetics, Combustion Calorimetry, and Quantum Chemical Computations Combined. *J. Am. Chem. Soc.* **2005**, *127*, 6116-6122.

18. Fu, Q.A.; Yang, J.L.; Wang, X.B. On the Electronic Structures and Electron Affinities of the *m*-Benzoquinone (BQ) Diradical and the *o*-, *p*-BQ Molecules: A Synergetic Photoelectron Spectroscopic and Theoretical Study. *J. Phys. Chem. A* **2011**,*115*, 3201-3207.
19. Horke, D. A.; Li, Q.; Blancafort, L.; Verlet. J. R. R. Ultrafast Above-Threshold Dynamics of the Radical Anion of a Prototypical Quinone Electron-Acceptor. *Nat. Chem*. **2013**, *5*, 711-717.
20. Chen, B.; Hrovat, D. A.; Deng, S. H. M.; Zhang, J.; Wang, X. B.; Borden, W. T. The Negative Ion Photoelectron Spectrum of meta-Benzoquinone Radical Anion ($MBQ^{\bullet-}$): A Joint Experimental and Computational Study. *J. Am. Chem. Soc.* **2014**, *136*, 3589-3596.
21. Hrovat, D.A.; Wang, X.B.; Borden, W.T. Calculations of the Relative Energies of the Low-lying Electronic States of 2,7-Naphthoquinodimethane and 2,7-Naphthoquinone. Substitution of Oxygen for CH_2 is Predicted to Increase the Singlet-triplet Energy Difference (ΔE_{ST}). *J. Phy. Org. Chem*. **2018**, e3824.
22. Yang, Z.; Hrovat, D. A.; Hou, G. L.; Borden, W. T.; Wang, X. B. Negative Ion Photoelectron Spectroscopy Confirms the Prediction of the Relative Energies of the Low-Lying Electronic States of 2,7-Naphthoquinone. *J. Phys. Chem. A* **2018**, *122*, 4838-4844.
23. Berson, J.A. in *Reactive Intermediate Chemistry*; Moss, R.S. Platz, M.S., Jones, M. Jr., Eds., Wiley Interscience, New Jersey, **2004**, p. 165.
24. Hrovat, D. A.; Wang, X.B.; Borden, W. T. Calculations on 1,8-Naphthoquinone Predict that the Ground State of this Diradical Is a Singlet. *J. Comput. Chem*. **2018** (https://doi.org/10.1002/jcc.25551).
25. Wang, X. B.; Wang, L. S. Development of a Low-temperature Photoelectron Spectroscopy Instrument Using an Electrospray Ion Source and a Cryogenically Controlled Ion Trap. *Rev. Sci. Instrum*. **2008**, *79*, 073108.

26. Hanstorp, D.; Gustafsson, M. Determination of the Electron Affinity of Iodine. *J. Phys. B: At., Mol. Opt. Phys.* **1992**, *25*, 1773-1783.

27. Wang, X. B.; Wang, L. S. Photodetachment of Free Hexahalogenometallate Doubly Charged Anions in the Gas Phase: $[ML6]^{2-}$, (M=Re, Os, Ir, Pt; L=Cl and Br). *J. Chem. Phys.* **1999**, *111*, 4497-4509.

28. Dunning, T.H. Gaussian Basis Sets for Use in Correlated Molecular Calculations. I. The Atoms Boron through Neon and Hydrogen. *J. Chem. Phys.* **1989**, *90*,1007-1023.

29. Kendall, R.A.; Dunning, T.H.; Harrison, R.J. Electron Affinities of the First-row Atoms Revisited. Systematic Basis Sets and Wave Functions. *J. Chem. Phys.* **1992**, *96*, 6796-6806.

30. Aquilante, F.; Autschbach, J.; Carlson, R. K.; Chibotaru, L. F.; Delcey, M. G.; De Vico, L.; Fdez. Galván, I.; Ferré, N.; Frutos, L. M.; Gagliardi, L.; et al. Molcas 8: New Capabilities for Multiconfigurational Quantum Chemical Calculations Across the Periodic Table. *J. Comput. Chem.* **2016**, *37*, 506-541.

31. Mozhayskiy, V.A., Krylov, A.I., ezSpectrum 3.0, see http://iopenshell.usc.edu/downloads (accessed April 2017).

32. Stanley, L. H.; Anstoter, C. S.; Verlet, J. R. R., Resonances of the Anthracenyl Anion Probed by Frequency-resolved Photoelectron Imaging of Collision-induced Dissociated Anthracene Carboxylic Acid. *Chem. Sci.* **2017**, *8*, 3054-3061.

TOC graphic

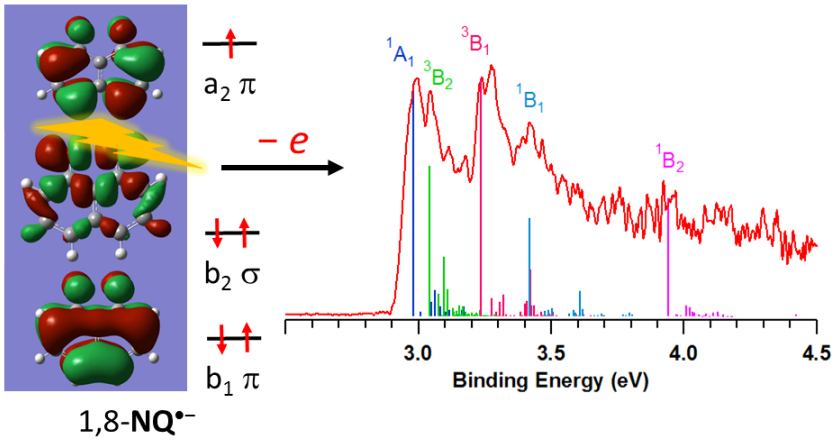
a2 π
− e
b2 σ
b1 π
1,8-NQ•−
1A1
3B2
3B1
1B1
1B2
3.0
3.5
4.0
4.5
Binding Energy (eV)